Investigation of depth selectivity of polarization gating for tissue characterization

Yang Liu, Young L. Kim, Xu Li, Vadim Backman

Biomedical Engineering Department, Northwestern University, Evanston, IL 60208
yangliu@northwesetern.edu

Abstract: Polarization gating has been widely used to selectively probe the structure of superficial biological tissue. However, the penetration depth selectivity of polarization gating has not been well understood. Using polarized light Monte Carlo simulations, we investigated how the optical properties of a scattering medium and light collection geometry affect the penetration depth of polarization gating. We show that, for a wide range of optical properties, polarization gating enables attaining a very shallow penetration depth, which is on the order of the mean free path length. Furthermore, we discuss the mechanisms responsible for this surprisingly short depth of penetration of polarization gating. We show that polarization-gated signal is generated primarily by photons emerging from the surface of the medium within a few mean free path lengths from the point of incidence.

References and Links

1. K. Sokolov, R. Drezek, K. Gossage, and R. Richards-Kortum, "Reflectance spectroscopy with polarized light: is it sensitive to cellular and nuclear morphology," Opt. Express **5**, 302-317 (1999), http://www.opticsexpress.org/abstract.cfm?URI=OPEX-5-13-302.
2. L. Nieman, A. Myakov, J. Aaron, and K. Sokolov, "Optical sectioning using a fiber probe with an angled illumination-collection geometry: evaluation in engineered tissue phantoms," Appl. Opt. **43**, 1308-1319 (2004).
3. A. Myakov, L. Nieman, L. Wicky, U. Utzinger, R. Richards-Kortum, and K. Sokolov, "Fiber optic probe for polarized reflectance spectroscopy in vivo: Design and performance," J. Biomed. Opt. **7**, 388-397 (2002).
4. S. L. Jacques, J. C. Ramella-Roman, and K. Lee, "Imaging skin pathology with polarized light," J. Biomed. Opt. **7**, 329-340 (2002).
5. S. L. Jacques, J. R. Roman, and K. Lee, "Imaging superficial tissues with polarized light," Lasers Surg. Med. **26**, 119-129 (2000).
6. Y. Kim, Y. Liu, R. K. Wali, H. K. Roy, M. J. Goldberg, A. K. Kromine, K. Chen, and V. Backman, "Simultaneous measurement of angular and spectral properties of light scattering for characterization of tissue microarchitecture and its alteration in early precancer," IEEE J. Sel. Top. Quantum Electron. **9**, 243-257 (2003).
7. S. P. Morgan and M. E. Ridgway, "Polarization properties of light backscattered from a two layer scattering medium," Opt. Express **7**, 395-402 (2000), http://www.opticsexpress.org/abstract.cfm?URI=OPEX-7-12-395.
8. J. R. Mourant, T. M. Johnson, S. Carpenter, A. Guerra, T. Aida, and J. P. Freyer, "Polarized angular dependent spectroscopy of epithelial cells and epithelial cell nuclei to determine the size scale of scattering structures," J. Biomed. Opt. **7**, 378-387 (2002).
9. V. Backman, R. Gurjar, K. Badizadegan, L. Itzkan, R. R. Dasari, L. T. Perelman, and M. S. Feld, "Polarized light scattering spectroscopy for quantitative measurement of epithelial cellular structures in situ," IEEE J. Sel. Top. Quantum Electron. **5**, 1019-1026 (1999).
10. R. R. Anderson, "Polarized-light examination and photography of the skin," Arch. Dermatol. **127**, 1000-1005 (1991).
11. J. M. Schmitt, A. H. Gandjbakhche, and R. F. Bonner, "Use of polarized-light to discriminate short-path photons in a multiply scattering medium," Appl. Opt. **31**, 6535-6546 (1992).
12. S. G. Demos and R. R. Alfano, "Optical polarization imaging," Appl. Opt. **36**, 150-155 (1997).
13. V. Backman, M. B. Wallace, L. T. Perelman, J. T. Arendt, R. Gurjar, M. G. Muller, Q. Zhang, G. Zonios, E. Kline, T. McGillican, S. Shapshay, T. Valdez, K. Badizadegan, J. M. Crawford, M. Fitzmaurice, S. Kabani,

H. S. Levin, M. Seiler, R. R. Dasari, I. Itzkan, J. Van Dam, and M. S. Feld, "Detection of preinvasive cancer cells," Nature **406**, 35-36 (2000).

14. H. K. Roy, Y. Liu, R. K. Wali, Y. Kim, M. J. Goldberg, A. K. Kromine, and V. Backman, "Four-dimensional elastic light scattering fingerprints as preneoplastic markers in the rat model of colon carcinogenesis," Gastroenterology **126**, 1071-1081 (2004).

15. A. Wax, C. H. Yang, M. G. Muller, R. Nines, C. W. Boone, V. E. Steele, G. D. Stoner, R. R. Dasari, and M. S. Feld, "In situ detection of neoplastic transformation and chemopreventive effects in rat esophagus epithelium using angle-resolved low-coherence interferometry," Cancer Res. **63**, 3556-3559 (2003).

16. L.-H. Wang, S. L. Jacques, and L.-Q. Zheng, "MCML - Monte Carlo modeling of photon transport in multi-layered tissues," Comput. Methods Programs Biomed. **47**, 131-146 (1995).

17. S. Bartel and A. H. Hielscher, "Monte Carlo simulation of the diffuse backscattering Mueller matrix for highly scattering media," Appl. Opt. **39**, 1580-1588 (2000).

18. F. Jaillion and H. Saint-James, "Description and time reduction of a Monte Carlo code to simulate propagation of polarized light through scattering media," Appl. Opt. **42**, 3290-3296 (2003).

19. M. J. Rakovic, G. W. Kattawar, M. Mehrubeoglu, B. D. Cameron, L. V. Wang, S. Rastegar, and G. L. Cote, "Light backscattering polarization patterns from turbid media: theory and experiment," Appl. Opt. **38**, 3399-3408 (1999).

20. X. Wang and L. Wang, "Propagation of polarized light in birefringent turbid media: A Monte Carlo study," J. Biomed. Opt. **7**, 279-290 (2002).

21. X. Wang, G. Yao, and L.-H. Wang, "Monte Carlo model and single-scattering approximation of polarized light propagation in turbid media containing glucose," Appl. Opt. **4**, 792-801 (2002).

22. G. Yao and L. V. Wang, "Propagation of polarized light in turbid media: simulated animation sequences," Opt. Express **7**, 198-203 (2000), http://www.opticsexpress.org/abstract.cfm?URI=OPEX-7-5-198.

23. B. C. Wilson and S. L. Jacques, "Optical reflectance and transmittance of tissues - principles and applications," IEEE J. Quantum Electron. **26**, 2186-2199 (1990).

24. D. Bicout, C. Brosseau, A. S. Martinez, and J. M. Schmitt, "Depolarization of multiply scattered waves by spherical diffusers - Influence of the size parameter," Phys. Rev. E **49**, 1767-1770 (1994).

25. V. Sankaran, M. J. Everett, D. J. Maitland, and J. T. Walsh, "Comparison of polarized-light propagation in biological tissue and phantoms," Opt. Lett. **24**, 1044-1046 (1999).

1. Introduction

Optical techniques have found a growing number of applications in biology and medicine. In particular, there has been a significant interest in using optical spectroscopy for early detection of precancer. In these applications, it is advantageous to probe the structure of superficial tissue since carcinomas derived from the epithelia are responsible for the majority of human cancers. Thus, depth-selective measurements are crucial to differentiate single and low-order scattering originating in the superficial tissue (e.g. epithelium) from the light multiply scattered in deeper tissue. Polarization gating, as a depth-selective technique, has been widely used to selectively probe the structures of superficial tissue based on the fact that multiple scattering depolarizes light [1-12]. Specifically, the sensitivity of the scattered light to near-surface structures can be increased by rejecting the depolarized diffusive light from the deeper tissue. The interest to polarization gating as a means to probe the morphology of superficial tissue in general and its alteration in neoplasia in particular is underscored by the fact that, compared to other depth-resolved techniques, polarization gating is simple and inexpensive [1-6, 8, 9, 13, 14]. Moreover, it can be combined with spectroscopic and scattering angle-resolved measurements [15] and allows *in vivo* implementation.

It has been previously shown that polarization gating enables selecting photons primarily scattered from very short tissue depths, i.e. only a few mean free paths below tissue surface. Despite the fact that the premise of polarization gating is straightforward (i.e. multiply scattered light looses its original polarization, whereas the polarization of short-traveling photons is retained), the mechanism that accounts for such *a priori* surprisingly short penetration depth has not been established [6, 9]. Moreover, detailed quantification of how tissue optical properties affect the penetration depth of polarization gating is still lacking. Thus, improved understanding of the effect of optical properties on the penetration depth of polarization-gated signals is important for a number of biomedical optics applications. This improved knowledge would allow investigators to locate the origins of polarization-gated

signals in tissue and associate them with specific tissue structures that can be assessed using polarization-gated measurements.

Several crucial questions remain unanswered: How do tissue optical properties affect the penetration depth? Although evidence exists that the differential polarization signal as well as the degree of polarization are sensitive to superficial tissue, the penetration depth has not been quantified. Can the penetration depth be controlled? Another important consideration is the effect of light collection geometry on the penetration depth of polarization gating. Although the relationship between the light collection geometry and penetration depth has been known in the diffusion regime, the effect of the collection geometry on polarization gating has not been completely understood, particularly given that a differentially polarized signal is expected to originate from short-traveling photons well beyond the diffusion regime. In many clinical applications, the design of the optical probe has to meet the clinical situation. For example, the imaging of skin pathology can be performed with relatively large illumination and light collection areas, up to a few centimeters in diameter; whereas spectroscopic measurements in gastrointestinal organs require small endoscope-compatible fiber-optic probes, which limit the area of illumination/collection to only a few hundreds of microns or a few millimeters. Does the penetration depth of polarization gating hold for different illumination and collection geometries?

In this paper, we present our detailed, quantitative investigation of polarization gating by means of polarized light Monte Carlo simulations. First, we confirm the short penetration depth selection achieved by polarization gating. Second, we quantify the effect of the optical properties of a scattering medium and light collection geometry on the penetration depth of polarization gating. Furthermore, we elucidate the mechanisms responsible for the surprisingly short depth of penetration of polarization gating. Finally, we discuss the implications of our findings on clinical applications.

2. Methods

2.1 Polarized light Monte Carlo simulations

We incorporated the polarization effect into the unpolarized multi-layered Monte Carlo code (Mcml) which was originally developed by Wang and Jacques [16]. Specifically, we implemented the algorithm developed by Rakovic et al., Bartel et al., Jaillion et al., Wang et al. and Yao et al [17-22]. In brief, the Stokes vector formalism is used to describe the polarization state of the photon packet. The Stokes vector of light scattered by particles is tracked throughout the photon propagation path. We modeled a scattering medium as a randomly uniform suspension of dielectric spherical particles of various diameters from 0.3 to 1.05 μm with refractive index of 1.59, which is typically used in these kinds of investigations. The probability of light scattering as a function of scattering angle θ and azimuthal angle ϕ was determined using Mie theory. The sampling of θ and ϕ was performed using an efficient algorithm developed by Jaillon et al [18]. For each backscattered photon, the spatial coordinates on the surface of the medium and the corresponding output Stokes elements were recorded and stored. The code has been validated by comparing our results with previously reported results [17, 18]. We used 2.5×10^7 photons in our simulations. As discussed below, the numerical experiments were designed to ensure that (1) the light collection geometry modeled in the simulations emulated realistic experimental conditions and (2) the output of the numerical simulations is analogous to those typically recorded in experiments.

2.2 Monte Carlo simulations of polarization gating

First, we define several parameters to facilitate further discussion. We use $p(r,\phi)$ to denote the probability of photons emerging from a scattering medium at radial distance r from the source (i.e. the point of incidence) per unit area, where ϕ is the azimuthal angle. $P(r,\phi) \equiv rp(r,\phi)$ is the probability of photons emerging from a scattering medium at radial distance r per unit length.

Second, we briefly review the principles of polarization gating [1-3, 5, 6, 9, 11]. In polarization gating, a polarized light illuminates a particular site on the surface of a sample, such as biological tissue, and the returned elastic scattering signal is split into two components with polarizations parallel (co-polarized signal $I_\parallel$) and orthogonal (cross-polarized signal $I_\perp$) to that of the incident light, respectively. The co-polarized signal is generated by both low-order scattering (primarily from scatterers located close to the surface) and multiple scattering (primarily from scatterers located deeper into the medium). On the other hand, the cross-polarized signal is predominantly generated by the multiply scattered photons from the deeper layers of the medium. Because multiple scattering depolarizes scattered light [5, 9, 11, 12], the sensitivity to the low-order scattering component can be increased by subtracting off the depolarized multiple scattering signal. This can be achieved by subtracting $I_\perp$ from $I_\parallel$. The resulting signal $\Delta I = I_\parallel - I_\perp$ is referred to as the differential polarization signal and predominately determined by the single and low-order scattering in the superficial layer of the scattering medium.

To investigate the penetration depth of polarization-gated signal, we designed a simple numerical experiment. We simulated light interaction with a single-layer tissue model, which was composed of uniformly distributed dielectric spherical particles from 0.3 to 1.05 μm with refractive index of 1.59. In order to avoid the effect of the reflection at the interface, we matched the refractive indices at the boundary of the layer under study. The rationale for the use of the single-layer model was not to mimic light reflectance from a thick tissue. Instead, we attempted to quantify the penetration depth of polarization gating by measuring the intensity of the reflected light as a function of model thickness and, as discussed below, elucidating the contribution of a given depth within a semi-infinite medium to the polarization-gated signal.

The numerical experiments followed the protocol of other laboratory experiments that demonstrated a short depth of penetration of polarization gating [6, 9]. In brief, we varied the geometrical thickness D of the sample and, thus, its optical thickness τ, which is defined as $\tau = (\mu_s + \mu_a)D$ where μ_s and μ_a are the scattering and absorption coefficients, respectively. For each D and τ, the co- and cross-polarized signals were recorded for various radii of collection R, i.e. $I_\parallel(\tau, R) = \int_{r=0}^{R} \int_{\phi=0}^{2\pi} P_\parallel(r,\phi)drd\phi$ and $I_\perp(\tau, R) = \int_{r=0}^{R} \int_{\phi=0}^{2\pi} P_\perp(r,\phi)drd\phi$.

As shown in Fig. 1(a), as τ increases, the differential polarization signal ($\Delta I(\tau, R = 3mm) = I_\parallel(\tau, R) - I_\perp(\tau, R)$) first increases and then reaches a plateau at $\tau_c \sim 3$. Here, the differential polarization signal is normalized by the maximum intensity for large τ. This curve is referred to as the *saturation curve*. Varying τ provides a simple yet efficient method for quantifying the contribution of different depths to the differential polarization signal. Indeed, $\Delta I(\tau) = \int_0^\tau C(\tau')d\tau'$, where $C(\tau)$ is the contribution of depth τ to the polarization-gated signal. The fact that the saturation curve $\Delta I(\tau)$ levels off after $\tau_c \sim 3$ indicates that the differential polarization signal is determined by scattering events occurring at $\tau < \tau_c$ and the contribution from the deeper scatterers to the differential polarization signal is negligible. For comparison, as shown in Fig. 1(b), for the same range of τ, the unpolarized light intensity $I_\parallel + I_\perp$ continues increasing without reaching a plateau, in agreement with previous experimental observations that unpolarized light has considerably greater penetration depth relative to that of the polarization-gated signal.

The comparison shown in Fig. 1 clearly indicates that polarization gating rejects photons propagating deep into the medium, which results in the saturation of $\Delta I(\tau)$ with τ. The saturation curve can be used as a convenient tool to analyze polarization gating. First, it provides a simple method to quantify the penetration depth. Here we define the penetration

depth T of differential polarization signal as the optical depth τ such that the saturation curve reaches 90% of its saturation value, i.e. ΔI is primarily generated by photons scattered within $\tau <$ T. Furthermore, we point out that $I_\parallel$ and $I_\perp$ obtained from the Monte Carlo simulations are the same quantities that are measured in polarization gating experiments. Therefore, the analysis based on our numerical simulations can be directly linked to the experimental data.
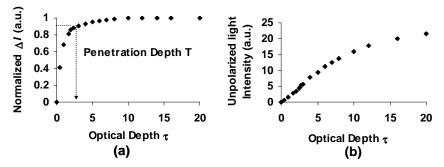

Fig. 1. Comparison of the saturation of (a) differential polarization and (b) unpolarized signals with the increase of the optical thickness τ of a scattering medium. (a) As τ increases, the normalized differential polarized intensity ΔI ($\Delta I(\tau, R = 3mm) = I_\parallel(\tau, R) - I_\perp(\tau, R)$) first increases and then reaches a plateau at $\tau_c \sim 3$. Optical depth τ is defined as $\tau = (\mu_s + \mu_a)D$ where D is the geometrical thickness and μ_s and μ_a are the scattering and absorption coefficients, respectively. (b) For comparison, unpolarized light signal $I_\parallel(\tau, R) + I_\perp(\tau, R)$ does not exhibit the saturation behavior until a much higher τ.

3. The effect of optical properties of the medium and light collection geometry on the depth selectivity of polarization gating

The penetration depth of polarization gating may depend on the optical properties of a medium as well as the light collection geometry. Understanding how the depth of penetration changes with tissue optical properties is central to many biomedical applications of polarization gating. In this section, we investigate the penetration depth as a function of scattering coefficient μ_s, absorption coefficient μ_a, and anisotropy factor g. In all simulations, all optical parameters were chosen to be within the physiological range [23]. In addition, the light collection geometry, which is often restricted by the clinical situation, may also have a significant effect on the depth of penetration. Therefore, we incorporate the effect of different light collection geometries, i.e., varying lateral range R, in our numerical studies presented in this section.

3.1 Effect of scattering coefficient

To investigate the effect of μ_s on the depth of penetration of polarization gating, we varied μ_s while keeping other optical parameters constant: $g = 0.809$ and $\mu_a = 0.1$ cm^{-1}. As discussed in Methods, we defined the depth of penetration of polarization-gated signal T as the optical depth τ ($\tau = (\mu_s + \mu_a)D$, where D is the physical penetration depth) such that the saturation curve reaches 90% of its saturation value. (Such normalization of T by the mean free path $l_s = 1/(\mu_s + \mu_a)$ is convenient, because, as discussed below, the physical penetration depth D is proportional to the optical depth, which scales with l_s.) Figure 2(a) shows the dependence of the penetration depth T on μ_s for different light collection radii R. The dimensionless parameter R/l_s' is used as the measure of the light collection geometry, where l_s' is the transport mean free path length defined as $l_s' = 1/(\mu_s(1-g))$. (The rationale for such normalization is primarily due to practical considerations: In an experiment, R is on the same

order of magnitude as l_s', which, in turn, is relatively easy to determine experimentally. Furthermore, for a given tissue type the range of l_s' is usually known. Given that l_s' characterizes the spatial extend of light propagation in tissue, experimentalists routinely compare the radius of light collection with l_s'.) As shown in Fig. 2(a), for a given R/l_s', the penetration depth is independent of μ_s, and falls within 1.5 - 2.7 range, as expected. This short penetration depth agrees well with the values previously reported from the experiments in biological tissue [1, 9]. (The corresponding physical penetration depth is equal to T/μ_s.) However, as further illustrated in Fig. 2(b), T does depend on R/l_s'. Specifically, the penetration depth increases with R/l_s'. This trend levels off for $R>l_s'$. For $R>>l_s'$, T is independent of either μ_s or R and approaches a limiting value of 2.7. The rationale for this behavior is discussed in section 4.
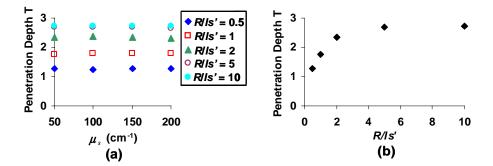

Fig. 2. Effect of μ_s and light collection geometry on the penetration depth of differential polarization signal T. (a) The dependence of T on μ_s for different light collection radii R, $\mu_a =$ 0.1 cm⁻¹ and $g = 0.809$. The dimensionless parameter R/l_s' is used as the measure of the light collection geometry, where l_s' is the transport mean free path defined as $l_s' = 1/(\mu_s(1-g))$. (b) The dependence of T on different R/l_s'.

3.2 Effect of absorption

Light absorption in tissue, which is governed by a number of endogenous absorbers including hemoglobin and melanin can affect light propagation in tissue. It is well known that in the diffusion regime, absorption shortens the depth of penetration of diffused light. However, the effect of absorption on the penetration depth of the differential polarization signal has not been investigated.

We varied μ_a within the physiological range from 0.01 to 10 cm⁻¹ while keeping the other optical parameters constant at $\mu_s = 200$ cm⁻¹ and $g = 0.809$. Figure 3 shows the dependence of the penetration depth of differential polarization signal on μ_a for different R/l_s'. For $R<l_s'$, T is essentially independent of μ_a. Indeed, for $R/l_s' = 0.5$, T~1.2 and changes only by 2% over a wide range of $\mu_a = 0.01$ - 10 cm⁻¹. On the other hand, for $R>l_s'$, T is somewhat dependent on μ_a. For instance, for $R/l_s' = 10$, T decreases by 10% when μ_a increases from 0.01 to 10 cm⁻¹. However, in the range of $\mu_a < 1$ cm⁻¹, T is independent of μ_a. For example, T decreases only by less than 1% when μ_a changes from 0.01 to 1 cm⁻¹. Furthermore, as illustrated in Fig. 3(b), the penetration depth increases with R/l_s'. This trend levels off for $R>>l_s'$ when T reaches its limiting value, which, in turn, depends on μ_a as discussed above.

3.3 Effect of anisotropy factor

The anisotropy factor g plays a crucial role in the light interaction with tissue. It typically varies from 0.8 to 0.95 for most biological tissue [23]. Here we investigate how the depth of

penetration depends on the anisotropy factor for various light collection geometries in the presence of weak and strong absorption.

Figure 4(a) demonstrates the effect of g on the penetration depth T for different R in the presence of weak absorption ($\mu_a = 0.1$ cm^{-1}, $\mu_s = 200$ cm^{-1}). In the case when $R/l_s'<1$, T is essentially independent of g. Indeed, within a wide range of $g = 0.65$-0.95, the penetration depth does not exceed 2. However, in case of a large area of light collection, e.g. $R/l_s'>2$, a different picture emerges: although for $g<0.9$ the depth of penetration is not sensitive to g, it rapidly increases with g for $g>0.9$.

Figure 4(b) compares the dependence of the penetration depth of polarization gating on the anisotropy factor in the case of weak ($\mu_a = 0.1$ cm^{-1}) and strong absorption ($\mu_a = 10$ cm^{-1}) for $R/l_s' =10$. Contrary to the case of weak absorption, where T is increased dramatically with g for $g>0.9$ and $R/l_s' >2$, in the case of strong absorption, T~1-3 and is much less sensitive to g for $g = 0.65$-0.95.
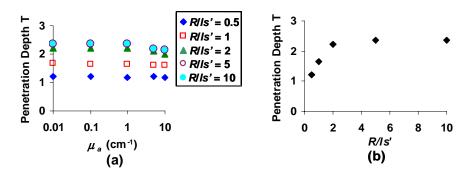

Fig. 3. Effect of μ_a and light collection geometry on the penetration depth of differential polarization signal T. (a) The dependence of T on μ_a and light collection radius R, $\mu_s = 200$ cm^{-1} and $g = 0.809$. (b) The dependence of T for different R/l_s' for $\mu_a = 0.1$ cm^{-1}.
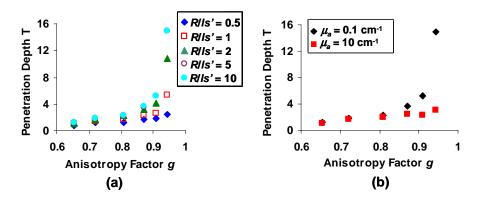

Fig. 4. Effect of g on the penetration depth of polarization gating for different light collection radii R in the presence of weak and strong absorption. (a) The dependence of the penetration depth on g and the light collection radius R in case of weak absorption ($\mu_a = 0.1$ cm^{-1}, $\mu_s = 200$ cm^{-1}). (b) Comparison of the effect of g on the penetration depth in the presence of weak ($\mu_a = 0.1$ cm^{-1}) and strong absorption ($\mu_a = 10$ cm^{-1}) for $R/l_s'=10$.

3.4 Summary

In summary, in this section, we investigated the effect of optical properties of a scattering medium and light collection geometry on the penetration depth of polarization gating. We

found that in a wide range of optical properties, the physical depth of penetration of polarization-gated signal is extremely shallow: it is primarily determined by the mean free path length and is less than $2l_s$, i.e. T<2 (Fig. 2(a)). Specifically, this conclusion holds if one of the following criteria is satisfied: $R<l_s'$, μ_a is not much smaller than μ_s, and g<0.9. These conditions are satisfied in many tissue optics applications. However, outside this domain, T may exceed the value of two: it increases with R, g, and $1/\mu_a$. In particular, T has only a weak dependence on either R or μ_a. Indeed, for g<0.9, T does not exceed the value of 3 for arbitrary R and μ_a. It is only in the case of highly forward-directed scattering (g>0.9), which applies only to certain tissue types including some types of epithelia, when the physical penetration depth is not limited by l_s any longer and substantially increased. In this case, if a short penetration depth is desirable, T can be reduced by choosing $R<l_s'$, as discussed above.

4. Discussion

The studies discussed in the previous section reveal that the polarization gating can be used to select short-traveling photons, and the penetration depth of polarization gating may depend on both the optical properties of the medium and light collection geometry. In this section, we discuss the mechanisms responsible for *a priori* surprisingly short depth of penetration of polarization-gated signal.

4.1 Relationship between the radial intensity distribution and the depth of penetration of polarization gating

The principle of polarization gating [5, 11, 12, 24] can be understood from the analysis of the radial intensity distributions $P_\parallel(r)$ and $P_\perp(r)$ of photons emerging from the surface. Figure 5(a) shows a typical example of the spatial intensity distributions for co-polarized, cross-polarized and differential polarized signals, $P_\parallel(r)$, $P_\perp(r)$ and $\Delta P(r) = P_\parallel(r)$ - $P_\perp(r)$, respectively, at g = 0.809, $\mu_s = 200$ cm^{-1} and $\mu_a = 0.1$ cm^{-1}. As evident from Fig. 5(a), for $r < l_s'$, which correspond to relatively short photon path lengths, the intensity of the co-polarized signal is much higher than that of the cross-polarized signals. This result indicates that the
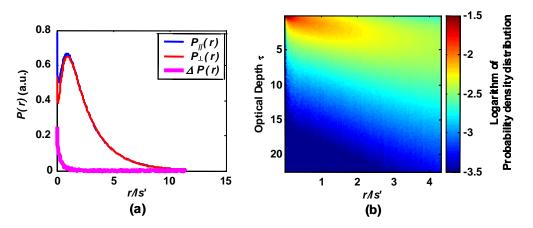

Fig. 5. The relationship between the radial intensity distribution and the optical depth. (a) Radial intensity distribution of co-polarized signal ($P_\parallel$(r)), cross-polarized signal ($P_\perp$(r)) and differential polarization signal (ΔP(r)) as a function of r/l_s' for g = 0.809, $\mu_a = 0.1$ cm^{-1} and $\mu_s = 200$ cm^{-1}. $P(r)$ is the probability of photons emerging from a scattering medium at radial distance r per unit length. $P(r) = rp(r)$ with $p(r)$ the probability per unit area. (b) Depth of penetration of scattered light correlates with its radial distribution (g = 0.809). The color intensity map represents the logarithm of the probability density distribution of photons as a function of penetration depth at each radial distance r.

polarization of photons emerging at short radial distance r from the point of incidence is mostly preserved, i.e. $P_{\parallel}(r) >> P_{\perp}(r)$. However, when $r > l_s'$, $P_{\parallel}(r) \sim P_{\perp}(r)$ and $\Delta P(r) \rightarrow 0$ (i.e. $\Delta P\ (r>l_s') << \Delta P\ (r<l_s')$), indicating that these photons have approximately equal probability of emerging from the tissue surface either in co-polarized or cross-polarized state. Thus, because $\Delta I(r) = \int_0^r \Delta P(r')dr'$, we conclude that the short depth of penetration of polarization gating is due to the fact that the differential polarization signal primarily selects photons emerging from the surface of the medium within only a few mean free path lengths from the point of incidence (Fig. 5(a)). In turn, such reduction of the effective collection area ensures that the photons contributing to the polarization-gated signal can emerge only from relatively short depths. Indeed, the relationship between the radial intensity distribution and the corresponding penetration depth is well known and further illustrated in Fig. 5(b). This color intensity map shows the logarithm of the probability density distribution of photons as a function of optical depth at each radial distance r. This figure clearly demonstrates that the photons emerging at a few mean free path lengths do not penetrate the medium deeper than a few l_s.

4.2 The effect of optical properties on the radial intensity distribution of polarization-gated signal

From the previous discussion it follows that if the short depth of penetration of polarization gating is due to the preferential selection of photons emerging from small radial distances, the effect of optical properties on the penetration depth of polarization gating discussed in Section 3 should also be reflected in the width of $\Delta P(r)$. Here the width of $\Delta P(r)$, R_c, is defined as the radial distance from the source that corresponds to 90% area under the curve, i.e. $\int_0^{R_c} \Delta P(r)dr \left/ \int_0^{\infty} \Delta P(r)dr \right. = 0.9$. It is more informative, however, to express the width of $\Delta P(r)$ as a dimensionless quantity $W = R_c(\mu_s + \mu_a)$. We note that W is directly related to and responsible for the depth of penetration of polarization-gated signal. (Thus, W is normalized by l_s.) Figure 6 shows the width of the radial intensity distribution of differential polarization signal as a function of μ_s (Fig. 6(a)), μ_a (Fig. 6(b)) and g (Fig. 6(c)). As expected, these trends are analogous to those of the penetration depth (Figs. 2-4). Specifically, W is independent of μ_s, decreases with μ_a and increases with g. Furthermore, Fig. 7 shows an excellent linear correlation between W and T for different combinations of optical parameters.

The shallow depth of penetration of polarization gating (e.g. on the order of a mean free path length) is due to the fact that polarization-gated signal is generated primarily by photons emerging from the medium within only a few mean free paths. Thus, polarization gating effectively reduces the light collection area and, hence, preferentially selects short-traveling photons. The optical or experimental conditions that reduce W also result in a shorter penetration depth. The effect of μ_a, μ_s, g, and R on the depth of penetration of polarization gating can be understood based on how these parameters affect the width of $\Delta P(r)$. In particular, the width of $\Delta P(r)$ is independent of μ_s, and, therefore, scattering coefficient does not affect the optical penetration depth. On the other hand, higher absorption attenuates long photon paths and, thus, reduces the width of $\Delta P(r)$ as well as T. Moreover, in a highly forward scattering regime ($g>0.9$), polarization is preserved for longer light paths [25], which increases both the width of $\Delta P(r)$ and T. Finally, the effect of light collection radius R on T can be viewed as due to the dependence W on R. For $R>l_s'$, W is essentially independent of R and, thus, T does not change with R. On the other hand, for $R<l_s'$, W is approximately proportional to R, and the depth of penetration can be controlled by choosing an appropriate R.
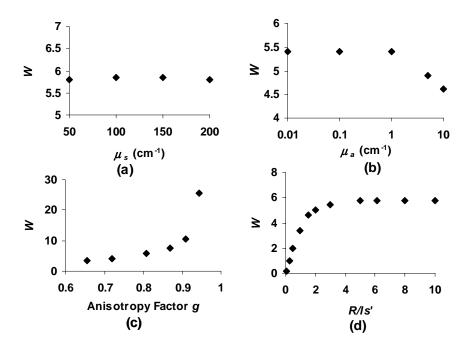
Fig. 6. The effect of optical properties of a scattering medium and light collection geometry on the radial intensity distribution of the differential polarization signal. (a) The effect of μ_s on the width of the radial intensity distribution of differential polarization signal, W ($\mu_a = 0.1$ cm^{-1} and $g = 0.809$). (b) The effect of μ_a on the width of the radial intensity distribution ($\mu_s = 200$ cm^{-1}, $g = 0.809$). (c) The effect of g on the width of the radial intensity distribution ($\mu_s = 200$ cm^{-1} and $\mu_a = 0.1$ cm^{-1}). (d) The relationship between light collection radius R/l_s' and the width of the radial intensity distribution ($\mu_s = 200$ cm^{-1}, $\mu_a = 0.1$ cm^{-1} and $g = 0.809$).
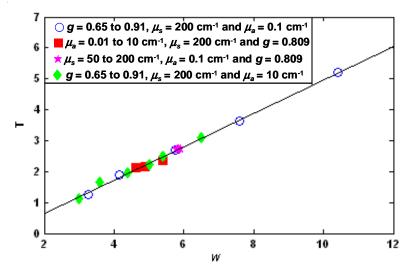

Fig. 7. The width of radial intensity distribution W has an excellent linear correlation with the penetration depth of polarization-gated signal T for different combinations of optical parameters including $\mu_s = 50$-200 cm^{-1}, $\mu_a = 0.01$-10 cm^{-1}, and $g = 0.65$-0.91.

5. Conclusion

In this paper, we utilized polarized light Monte Carlo simulations to investigate the depth selectivity of polarization gating and its dependence on the optical properties of scattering media as well as light collection geometry. Our numerical experiments show that for a wide range of optical properties, polarization gating enables attaining a very shallow penetration depth, which is on the order of the mean free path. This conclusion holds if one of the following criteria is satisfied: $R<l_s'$, μ_a is not much smaller than μ_s, and $g<0.9$. These conditions are satisfied in many tissue optics applications. However, outside this domain the penetration depth of polarization gating increases with R, g, and $1/\mu_a$. We found that the penetration depth has a relatively weak dependence on either R or μ_a. Although the effect of g is more pronounced, it is only in the case of highly forward-directed scattering ($g>0.9$), which applies only to a few specialized tissue types, when the penetration depth is not limited by l_s any longer and substantially increased. In this case, if a short penetration depth is desired, it can be reduced by limiting the area of light collection to $R<l_s'$.

Furthermore, we identified the potential mechanism responsible for the depth-selectivity of polarization gating. Our numerical experiments indicate that polarization gating effectively reduces the light collection area, so that its radial extend is on the order of a few mean free paths, and, thus, preferentially selects short-traveling photons. In other words, the use of polarization gating is analogous to the reduction of the scattered light collection area.

These findings may guide future clinical applications of polarization gating. For example, endoscope-compatible fiber-optic probes are widely used to probe gastrointestinal tissue *in vivo*. The size of such probes is restricted to a few hundreds of microns or a few millimeters. In this particular scenario, the penetration depth of differential polarization signal is not expected to depend strongly on the specifics of the optical properties of tissue and is on the order of one mean free path, which is in good agreement with the previously reported values [1, 6, 9]. On the other hand, in the wide-area tissue imaging, such as skin pathology imaging, the radius of light collection can be as large as a few centimeters. In this case, the tissue optical properties may have significant effect on the penetration depth.

Acknowledgments